

INTERIM
1N-46-CP
14 CIT.
98118

U. S. PARTICIPATION IN THE GOME AND SCIAMACHY PROJECTS

NASA Grant NAGW-2541

Annual Progress Report No. 4

For the period 1 April 1995 through 31 March 1996

Principal Investigator:

K.V. Chance
Smithsonian Astrophysical Observatory

October 1996

Prepared for
National Aeronautics and Space Administration

Smithsonian Institution
Astrophysical Observatory
Cambridge, Massachusetts 02138

The Smithsonian Astrophysical Observatory
is a member of the
Harvard-Smithsonian Center for Astrophysics

The NASA Technical Officer for this grant is Dr. Jack Kaye
Code SED, NASA/HQ

**Annual Report
Progress Through March 31, 1996**

**NASA Grant NAGW-2541
U. S. Participation in the GOME and SCIAMACHY Projects**

**Principal Investigator:
K. V. Chance
Smithsonian Astrophysical Observatory
Cambridge, MA 02138**

**Co-Investigator:
J. C. Geary
Smithsonian Astrophysical Observatory
Cambridge, MA 02138**

Introduction

This report summarizes research done under NASA Grant NAGW-2541 from April 1, 1995 through March 31, 1996. The research performed during this reporting period includes development and maintenance of scientific software for the GOME retrieval algorithms, consultation on operational software development for GOME, further sensitivity and instrument studies to help finalize the definition of the SCIAMACHY instrument, and consultation on optical and detector issues for both GOME and SCIAMACHY. The Global Ozone Monitoring Experiment was successfully launched on the ERS-2 satellite on April 20, 1995, during this reporting period, and is working in the expected fashion. The European Space Agency has made their selections from responses to the Announcement of Opportunity for GOME validation and science studies, part of the overall ERS AO. The Smithsonian Astrophysical Observatory (SAO) proposal has been selected. These proposals are primarily for access to the data; ESA does not provide research funding for the selected investigations. The SAO activities that are carried out as a result of selection by ESA are funded by the present grant, to the limit that can be accomplished at the present level of funding. SCIAMACHY is currently in Phase C/D. Instrument design is almost finalized and selection of infrared detectors from the initial production run has been made. A new development in these programs is the initial discussion of a series of European ozone monitoring instruments (OMI) based, to an extent that is currently under discussion, on

GOME. These will fly on the Metop series of operational meteorological satellites being planned by Eumetsat. K. Chance is the U.S. member of the OMI Users Advisory Group.

GOME and SCIAMACHY Studies Through March 1996

The research at the SAO for the GOME and SCIAMACHY projects includes development and maintenance of scientific software for the GOME retrieval algorithms, advising and assisting in the development of GOME operational software, participation in GOME validation and science studies, further sensitivity and instrument studies to help finalize the definition of the SCIAMACHY instrument, further development of the SCIAMACHY study to produce the Scientific Requirements Document for Data and Algorithm Development, development of scientific software for SCIAMACHY retrievals, and consultation on optical and detector issues for both GOME and SCIAMACHY.

GOME

The development of the scientific code that will implement the GOME retrieval algorithms and, eventually, their realization as operational processing code, is well underway. This code will evolve into SCIAMACHY code by incorporating appropriate infrared line-by-line and ESF-based band-model forward modeling capability and the limb and occultation measurement geometries of SCIAMACHY. Given the accelerated schedule for GOME development, we have concentrated on those aspects that are specific to the GOME project. SAO GOME studies to date include the following items:

- Guiding the development of GOME Level 0-1 and 1-2 operational software through extensive collaboration with the DLR.
- Further investigation of cloud studies, leading to a paper, "Analysis of cloud-top height and cloud coverage from satellites using the O₂ A and B bands," A. Kuze and K. Chance, *J. Geophys. Res.* **99**, 14,481-14,491 (1994). These studies included investigation of fitting schemes and analysis of uncertainties due to various error sources, including line parameters of O₂. They also resulted in production of the prototype operational algorithm for GOME cloud correction which has now been implemented in the Level 1 operational software.
- Substantial improvements to the GOMEware for thorough scientific testing of GOME algorithms, including those that are being implemented initially and those that are under

development. This includes the implementation of the SBUV code in the GOMEware, and its testing for a variety of simulated GOME measurements, and preliminary steps for inclusion of the GOMEtran finite-difference method forward model.

- Participation in GOME validation and scientific studies. The SAO proposal in response to the ESA Announcement of Opportunity for the ERS mission, which has now been selected, is included as Appendix A to this proposal. K. Chance is now a "GOME Validation Principal Investigator." Note that the validation studies include the first ozone profiles and tropospheric ozone abundances, which will be produced as off-line scientific products.
- Collaboration on the development of the DOAS method as the operational procedure for GOME Level 1-2 processing to produce O₃ columns from GOME. This collaboration includes code development, measurement window selection, and a number of related issues.
- Changes to operational code for GOME Level 0-2 processing, to adjust for post launch conditions and to correct initial deficiencies.
- Participation in GOMEtran forward model development, in collaboration with the University of Bremen.
- Spectroscopic and aerosol database development, including the production of an improved database of molecular parameters for the visible O₂ A band.
- Radiative transfer studies related to wavelength calibration and spatial and spectral aliasing, including development of an improved solar reference spectrum for wavelength-specific application.
- Improved determination of the wavelength-dependent Rayleigh scattering cross section.
- Improved molecular parameters for the Ring effect through molecular physics studies employing the best currently available molecular data; improved atmospheric cross sections describing the Ring effect.
- Participation in the ESA cloud and aerosol *ad hoc* study group to produce cloud and aerosol data products from GOME.

SCIAMACHY

SCIAMACHY is a joint German/Netherlands program, with scientific participation from other European countries and, in the U.S., the SAO. It is included for launch aboard the ESA Envisat-1, currently planned for 1999.

The SCIAMACHY Science Advisory Group (SSAG) was formed, including K. Chance of the SAO as a U.S. member and head of the Data and Algorithm Subcommittee, and J. Geary of the SAO as the other U.S. member and advisor on instrument and detector issues. The SSAG has met several times during the past year in order to address the many issues involved in the development of SCIAMACHY. SAO SCIAMACHY studies to date include the following items:

- Further definition of SCIAMACHY instrument, including: consultation on SCIAMACHY detector, cooling and instrumentation issues; finalization of the SCIAMACHY band definitions and detector selection criteria; synthetic retrieval studies for atmospheric spectroscopy in the infrared contributing to these definitions.
- Chairing the scientific working subgroup for Algorithm Development and Data Usage, including organization of joint GOME/SCIAMACHY science workshops and heading the development of a Scientific Requirements Document for SCIAMACHY Data and Algorithm Development.
- Radiative transfer studies, including acquisition of AVIRIS data for determination of infrared albedos for a number of measurement locations.
- Initial extension of the GOME software development to SCIAMACHY. In particular, this requires the inclusion of limb and occultation geometries, and extension into the infrared. Comparison of line-by-line forward modeling code with ESF band-model calculations is in progress at the University of Bremen, with SAO participation. Some preliminary database issues involved in this development have been addressed. The issue of properly combining limb and nadir measurements must be addressed in conjunction with the development of the SCIAMACHY observational strategy. This is being addressed in the context of the Algorithm Development and Data Usage subgroup.
- Contributions to the SCIAMACHY Instrument Requirements Document
- Contributions to the SCIAMACHY Scientific Requirements Document
- Production of the draft Scientific Requirements Document for SCIAMACHY Data and Algorithm Development.

- Participation in the definition of near real time data products for SCIAMACHY.
- Preliminary work on the Basic Infrared Absorption Spectroscopy (BIAS) technique for application to the SCIAMACHY infrared channels.

Publications from this Research Program Through March 1996

- 1990 SCIAMACHY Instrument Design, A. P. H. Goede, H. J. M. Aarts, C. van Baren, J. P. Burrows, K. V. Chance, R. Hoekstra, E. Hölzle, W. Pitz, W. Schneider, C. Smorenberg, H. Visser, and J. de Vries, *COSPAR XXVIII Plenary meeting*, paper S.1.6.12,
- 1990 GOME and SCIAMACHY: Remote Sensing of Stratospheric and Tropospheric Trace Gases, J. P. Burrows, W. Schneider and K. V. Chance, *CEC Air Pollution Report 34: Polar Stratospheric Ozone. Proceedings of the First European Workshop*, ed. J. A. Pyle and N. R. P. Harris, 99-102, ISBN2-87263-060-0.
- 1990 Database Needs for UV/Visible Spectroscopy, K. V. Chance, J. P. Burrows, R. Meller, G. K. Moortgat, D. Perner and W. Schneider, Paper 6.8, pp. 186-194, Proceedings of the 1990 Atmospheric Spectroscopy Applications Workshop, Moscow, U.S.S.R., ed. A. Barbe, Yu. N. Ponomarev and R. Zander, Published by Institute of Atmospheric Optics, Tomsk, U.S.S.R., Zak. 151-100-90.
- 1991 Retrieval and Molecule Sensitivity Studies for the Global Ozone Monitoring Experiment and the SCanning Imaging Absorption spectrometer for Atmospheric CHartographY, K. V. Chance, J. P. Burrows, and W. Schneider, *Proc. S.P.I.E., Remote Sensing of Atmospheric Chemistry*, 1491, 151-165.
- 1991 Scanning Imaging Absorption Spectrometer for Atmospheric ChartographY, J. P. Burrows and K. V. Chance, *Proc. S.P.I.E., Future European and Japanese Remote Sensing Sensors and Programs*, 1490 146-154.
- 1992 SCIAMACHY and GOME: The Scientific Objectives, J. P. Burrows and K. V. Chance, *S.P.I.E. Meeting on Optical Methods in Atmospheric Chemistry*, Berlin, Germany.
- 1992 GOME Instrument Simulation, A.P.H. Goede, C.J.Th. Günsing, T.M. Kamperman, J. de Vries, R.J. Spurr, J. P. Burrows and K. Chance, *S.P.I.E. Meeting on Optical Methods in Atmospheric Chemistry*, Berlin, Germany.
- 1992 Ozone Profile Retrievals from the ESA GOME Instrument, R. Munro, B. J. Kerridge, J. P. Burrows, and K. Chance, *1992 Quadrennial Ozone Symposium*.

- 1992 A Study of the Accuracy of Atmospheric Trace Gas Vertical Profile Retrieval from Satellite-based Occultation Measurements, J. P. Burrows, V. V. Rozanov, Yu. M. Timofeyev, A. V. Polyakov, R. J. D. Spurr and K. V. Chance, *Proceedings of the 1992 International Radiation Symposium*, Tallinn, Estonia.
- 1993 *Global Ozone Monitoring Experiment Interim Science Report*, J. P. Burrows, K. V. Chance, A. P. H. Goede, R. Guzzi, B. J. Kerridge, C. Muller, D. Perner, U. Platt, J.-P. Pommereau, W. Schneider, R. J. Spurr, and H. van der Woerd, ed. T. D. Guyenne and C. Readings, Report ESA SP-1151, ESA Publications Division, ESTEC, Noordwijk, The Netherlands, ISBN 92-9092-041-6.
- 1994 Analysis of Cloud-Top Height and Cloud Coverage from Satellites Using the O₂ A and B Bands, A. Kuze and K. V. Chance, *Journal of Geophysical Research* 99, 14,481-14,491.
- 1996 O₂ A Band Studies for Cloud Detection and Algorithm Improvement, K. Chance, *Proceedings of the GOME Geophysical Validation Campaign*, 65-68, European Space Agency Publication WPP-108.
- 1996 Ring Effect Studies: Rayleigh Scattering, Including Molecular Parameters for Rotational Raman Scattering, and the Fraunhofer Spectrum, K. Chance and R.J.D. Spurr, *Proceedings of the GOME Geophysical Validation Campaign*, 69-74, European Space Agency Publication WPP-108.
- 1996 GOME Calibration and Validation Using Backscatter UV Techniques, E. Hilsenrath, J. Gleason, S. Janz, X-y Gu, R.P. Cebula, K. Chance, and R. Hoekstra, *Proceedings of the GOME Geophysical Validation Campaign*, 85-91, European Space Agency Publication WPP-108.

51-46
98141

246189
48

O₂ A BAND STUDIES FOR CLOUD DETECTION AND ALGORITHM IMPROVEMENT

K. Chance

Harvard-Smithsonian Center for Astrophysics
Cambridge, MA, USA

Abstract

Detection of cloud parameters from space-based spectrometers can employ the vibrational bands of O₂ in the $b^1\Sigma_g^+ \leftarrow X^3\Sigma_g^-$ spin-forbidden electronic transition manifold, particularly the $\Delta v = 0$ A band. The GOME instrument uses the A band in the Initial Cloud Fitting Algorithm (ICFA). The work reported here consists of making substantial improvements in the line-by-line spectral database for the A band, testing whether an additional correction to the line shape function is necessary in order to correctly model the atmospheric transmission in this band, and calculating prototype cloud and ground template spectra for comparison with satellite measurements.

and R25R25 lines, which are blended together. The measurements also include air broadening studies for a selection of 5 lines. They find "roughly a 3% increase in broadening for air over pure O₂," although their Table II appears to indicate more like a 2% increase. Their 3% is adopted here, with a 2% uncertainty. The temperature dependence of the self broadening was measured for 24 lines, from P29P29 through R5R5, over the temperature range +100 to -20° C. The temperature coefficient, n , for the pressure broadening coefficients, determined for the ensemble of lines measured, is 0.76(5), where $(\gamma(T) = \gamma(T_0) \times (T_0/T)^n)$. This compares with the $\bar{n} = 0.72$ that can be obtained from the very limited data set assembled in Chance *et al.* [1991].

1. SUMMARY OF NEW LABORATORY MEASUREMENT DATA

The new measurements incorporated into the present work are from Ritter [1986] and Ritter and Wilkerson [1987] (together, RW). They include improved measurements of line intensities, giving an overall band intensity that is 15% larger than the previous measurements that are the source of the parameters in the current HITRAN listing [Miller *et al.*, 1969; Rothman *et al.*, 1992]. It is worth noting that the uncertainties in Miller *et al.* [1969] are given as 4%, while those of RW are 2%. The level of disagreement (arguably just a bit worse than 2σ) is an indication of how difficult these seemingly straightforward measurements actually are. RW also include self-broadening measurements of the linewidths, which are on the average 8% smaller than the current air broadening values in HITRAN (the HITRAN values actually come from measurements in the B band [Giver *et al.*, 1974], which were substituted for A band widths for lack of specific A band measurements (see Kuze and Chance [1994])). The RW measurements are made at 294 K, for lines up to P29P29 in the P branch and R27R27 in the R branch, except for the R21Q22

Estimated (2σ) final uncertainties for the measurements are:

1. Intensity: 2%; directly from the RW band strength.
2. Pressure broadening coefficients: 2%; from 294 K individual line uncertainties (small), plus the N₂/O₂ correction (the dominant term).
3. n : 7%; directly from measurements, $\bar{n} = 0.76(5)$. This corresponds to less than 2% uncertainty in the broadening coefficient for the range of temperatures encountered in the lower and middle atmosphere. The root-sum-square of the various error terms in pressure broadening is 3%.

The data measured by Ritter and Wilkerson can be extended to provide updated coefficients for use in cloud determination to replace the ones currently included in HITRAN [Rothman *et al.*, 1992], which were shown by Kuze and Chance [1994] to be insufficiently accurate for satellite-based cloud detection.

Processing of the Ritter and Wilkerson data to provide a more complete data set is accomplished as follows:

1. Pressure broadening coefficients for the lines omitted due to interference are replaced by those with the same N', N'' : $R21Q22$ and $R25R25$ are replaced by $R21R21$ and $R25Q26$.
2. O_2 pressure broadening coefficients measured by RW are multiplied by 1.03, to give air broadening. Coefficients for lines measured by RW in the $v = 0 \leftarrow 0$ band are also applied to the respective lines in the $v = 1 \leftarrow 1$ hot band and the $v = 0 \leftarrow 0$ band of $^{18}O^{16}O$. Hitran lines not measured by RW are multiplied by $1.03 / 1.09009 = 0.94488$, where 1.09009 is the average ratio of the RW measurements to the HITRAN coefficients.
3. The isotopic abundances are taken to be the those used in HITRAN, so that $^{16}O_2$ is 99.52% and $^{18}O^{16}O$ is 0.40%.
4. Intensity values for the three sub-bands are calculated starting with the 294 K band strength of RW, correcting the hot band by the Boltzmann factor of the band origin (1556.385 cm^{-1}) and the minor isotopic band by the appropriate isotopic ratio. The line intensities are translated to 296 K by explicitly calculating the rotation-spin partition functions using the term values from HITRAN and correcting for the RW approximation for the 294 K partition function of the major band.
5. In order to calculate individual line intensities, to supplement the measured ones, it is necessary to use the appropriate intensity formulas, which take into account the spin-rotation and spin-spin interactions [RW; Watson, 1968]. For the $v = 0 \leftarrow 0$ band of $^{16}O_2$ measured by RW the molecular constants from Albritton *et al.* [1973] are used, to be consistent, although better constants are now available from Mizushima *et al.* [1984] (and references cited therein). These latter constants are used to calculate the individual line intensities for the $v = 1 \leftarrow 1$ band of $^{16}O_2$ and the $v = 0 \leftarrow 0$ band of $^{18}O^{16}O$.

The final database derived from these calculation is available from the author via ftp.

2. TESTING OF LINE SHAPES, INCLUDING LINE NARROWING COEFFICIENTS
RW determined that the data as measured under laboratory conditions at high spectral resolution

($< 10^{-4} cm^{-1}$) were fitted better by including narrowing of the line core (Dicke narrowing) in the line shape function. Several line shapes were tested, including the Galatry line shape [Galatry, 1961]. It was found that all of the tested line shapes which included line narrowing provided superior fits to those using the Voigt profile, and that all were equivalent, to within experimental uncertainty. The Galatry profile was adopted for the bulk of the work because of the relative simplicity in implementing it [Varghese and Hanson, 1984]. RW found that all of the lines in the $O_2 A$ band can be reasonably described by a line narrowing coefficient of 0.0145 $cm^{-1} atm^{-1}$ (see RW for the exact definition of the coefficient in terms of the Galatry profile). An improved method for generating Galatry line profiles, employing the fast Fourier transform (FFT), has since been developed by Ouyang and Vargese [1985] (OV). These authors have distributed a version of their FFT computer code, which was used in the present study for investigation of the effect of line narrowing on the atmospheric O_2 absorption. In order to use the code, it was necessary to update it and streamline it somewhat. The FFT routine used in the code is from the International Mathematical and Statistical Library (IMSL); however, calls were to an outdated version of IMSL, which is no longer supported at our institution (nor, presumably, at most others). Therefore, the code was updated to IMSL Version 10. The updated version of the Galatry line profile code is available from the author via ftp. Implementation of this code and atmospheric investigation for the $O_2 A$ band proceeded as follows:

1. The OV code was compared in the Voigt limit against our standard Voigt subroutine (based upon algorithm 363 of the Collected Algorithms from CACM), which has an accuracy of 10 significant figures, for the case where the Lorentz half-width at half-maximum is 3.0 times the Gaussian half-width at $1/e$ intensity. The maximum disagreement was 0.13%; the maximum disagreement relative to the line center intensity was 0.06%. This was accepted as validation that the OV code can be properly used to assess the importance of line narrowing on the atmospheric O_2 spectrum.
2. Comparisons were made using the OV code with and without line narrowing for cases corresponding to the $O_2 A$ band at 5 and 10 km altitudes in the atmosphere, using pressure and temperature values from the US Standard Atmosphere [1976]. In the 5 km case, the maxi-

imum relative error in the line shapes is 1.8%; differences go to <1% by 2.9 Gaussian 1/e widths from line center. In the 10 km case, the maximum relative error is 2.4%; differences go to <1% by 2.5 Gaussian 1/e widths from line center. In both cases, the integral of differences over the line shapes is zero to within the accuracy of the single precision calculations. In the atmosphere, these differences will be in the saturated central parts of the lines for all but the weakest lines. Differences greater than 1% are all within 0.02 GOME pixel (for example) so they will not be visible in the spectra. Thus, the effect of line narrowing should be totally negligible, and we should be able to simply use the Voigt profile for satellite-based cloud correction.

3. SAMPLE O₂ A BAND CLOUD CORRECTION TEMPLATES FOR GOME

For initial comparisons with the GOME satellite data sample ground and 400 mbar cloud template spectra are calculated using a 16-layer atmosphere based upon the U.S. Standard Atmosphere [1976] and employing Version 5 of the GOME key data for wavelength calibration and for the GOME compound hyperbolic slit function:

$$y = \frac{a_1^2}{(x-x_0)^2 + a_0^2} + \frac{a_2^2}{(x-x_0)^4 + a_0^2} + \frac{a_3^2}{(x-x_0)^6 + a_0^2}$$

where y is the normalized spectral response and x is the spectral position in pixel number. The current slit function values are $a_0 = 0.7334$, $a_1 = 0.0756$, $a_2 = 0.4689$, and $a_3 = 0.5589$. The calculations are made for a solar zenith angle of 60° and a viewing angle of 22°, for a total (typical) path multiplier of 3.07853, as initially used in the Initial Cloud Fitting Algorithm (ICFA) of GOME. Figure 1a is the sample ground template, *i.e.*, the measured spectrum for light reflected back from ground level (1013.25 mbar). Figure 1b is the sample template for reflection from a cloud surface at 400 mbar. Figure 1c compares the shapes of the two templates to provide some feeling for the information available in distinguishing the relative level of light penetration from satellite spectra.

4. REFERENCES

D. L. Albritton, W. J. Harrop, and A. L. Schmeltekopf, Resolution of the discrepancies concerning the optical and microwave values for B₀ and

D₀ of the X³Σ_g⁻ state of O₂, *J. Molec. Spectrosc.* **46**, 103-118, 1973.

K. V. Chance, W. A. Traub, K. W. Jucks, and D. G. Johnson, On the use of O₂ spin-rotation lines for elevation angle calibration of atmospheric thermal emission spectra, *Int. J. IR and MM Waves* **12**, 581-588, 1991.

L. Galatry, Simultaneous effect of Doppler and foreign gas broadening on spectral lines, *Phys. Rev.* **122**, 1218-1223, 1961.

L. P. Giver, R. W. Boese, and J. H. Miller, Intensity measurements, self-broadening coefficients, and rotational intensity distribution for lines of the Oxygen B band at 6880 Å, *J. Quant. Spectrosc. Radiat. Transfer* **14**, 793-802, 1974.

A. Kuze and K. V. Chance, Analysis of cloud-top height and cloud coverage from satellites using the O₂ A and B bands, *J. Geophys. Res.* **99**, 14,481-14,491, 1994.

J. H. Miller, R. W. Boese, and L. P. Giver, Intensity measurements and rotational intensity distribution for the oxygen A band, *J. Quant. Spectrosc. Radiat. Transfer* **9**, 1507-1517, 1969.

M. Mizushima, L. R. Zink, and K. M. Evenson, Rotational structure of ¹⁶O₂, ¹⁶O¹⁷O, and ¹⁶O¹⁸O (X³Σ_g⁻) from laser magnetic resonance spectra, *J. Molec. Spectrosc.* **107**, 395-404, 1984.

X. Ouyang and P. L. Varghese, A reliable and efficient program for fitting Galatry and Voigt profiles to spectral data on multiple lines, *Appl. Opt.* **28**, 1538-1545, 1989.

K.J. Ritter, A high resolution spectroscopic study of absorption line profiles in the A-band of molecular oxygen, Ph.D. Thesis, University of Maryland, 1986.

K.J. Ritter and T.D. Wilkerson, High-resolution spectroscopy of the oxygen A band, *J. Molec. Spectrosc.* **121**, 1-19, 1987.

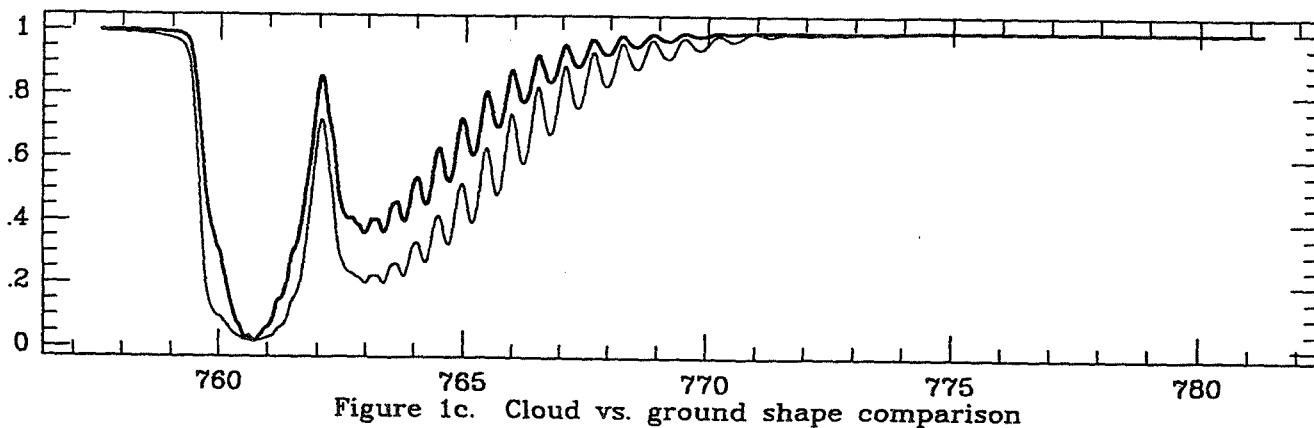
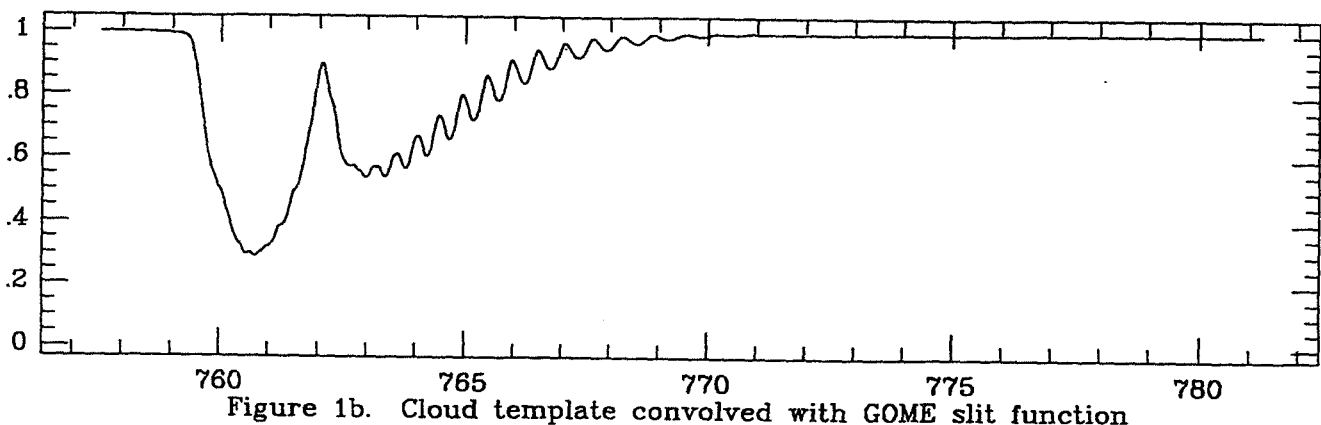
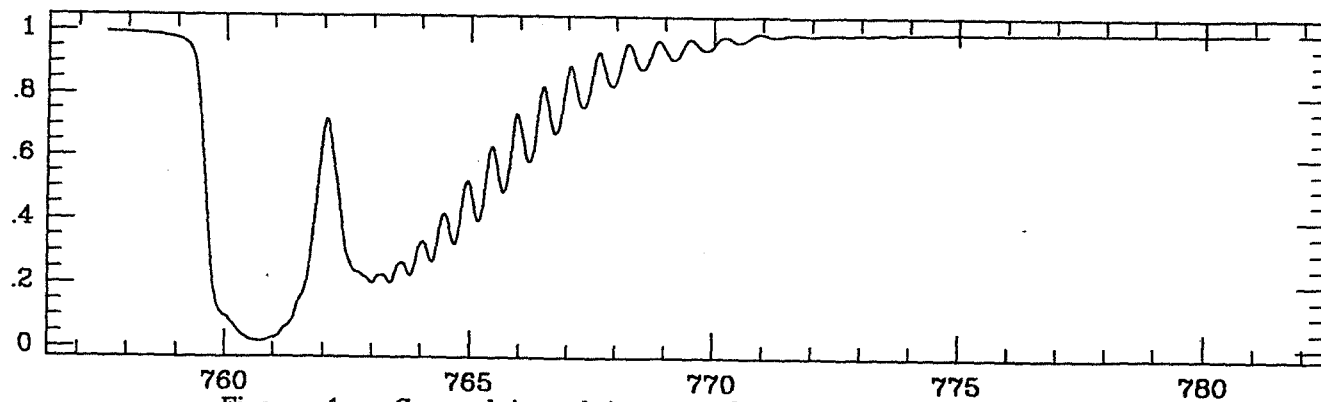
L. S. Rothman, R. R. Gamache, R. H. Tipping, C. P. Rinsland, M. A. H. Smith, D. C. Benner, V. M. Devi, J.-M. Flaud, C. Camy-Peyret, A. Perrin, A. Goldman, S. T. Massie, L. R. Brown, and R. A. Toth, The HITRAN molecular database editions of 1991 and 1992, *J. Quant. Spectrosc. Radiat. Transfer* **48**, 469-507, 1992.

"U.S. Standard Atmosphere Supplements, 1976," U.S. Government Printing Office, Washington, DC.

P. L. Varghese and R. K. Hanson, Collisional narrowing effect on spectral line shapes measured at high resolution, *Appl. Opt.* **23**, 2376-2385, 1984.

J. K. G. Watson, Rotational line intensities in $^3\Sigma-^1\Sigma$ electronic transitions, *Canad. J. Phys.* **46**, 1637-1643, 1968.

5. **ACKNOWLEDGEMENTS** This research was supported by NASA grant NAGW-2541.



52-46

98142 69

246190

C.P.

RING EFFECT STUDIES: RAYLEIGH SCATTERING, INCLUDING MOLECULAR PARAMETERS FOR ROTATIONAL RAMAN SCATTERING, AND THE FRAUNHOFER SPECTRUM

K. Chance and R.J.D. Spurr

Harvard-Smithsonian Center for Astrophysics
Cambridge, MA, USA

Abstract

Improved parameters for the description of Rayleigh scattering in air and for the detailed rotational Raman scattering component for scattering by O₂ and N₂ are presented for the wavelength range 200-1000 nm. These parameters enable more accurate calculations of bulk molecular scattering and of the "Ring effect" for a variety of atmospheric radiative transfer and constituent retrieval applications. A solar reference spectrum with accurate absolute vacuum wavelength calibration, suitable for convolution with the rotational Raman spectrum for Ring effect calculations, has been produced and is briefly described. The solar-rotational Raman convolved product is available for fitting of atmospheric spectra.

1. INTRODUCTION

The phenomenon that has come to be known as the "Ring effect" was first noted by Grainger and Ring [1962] as a filling in (broadening and reduction of depth) of solar Fraunhofer lines when viewed from the ground in scattered sunlight. Various processes have been proposed as contributing to the effect including scattering with fluorescence from aerosols and from the ground [Noxon and Goody, 1965; Hunten, 1970]. The predominance of molecular scattering as the major cause was established by Kattawar *et al.* [1981], who analyzed the Ring effect contributions from rotational Raman scattering and inelastic Rayleigh-Brillouin scattering. The Rayleigh-Brillouin contribution arises from the Doppler effect due to relative motion of the atmosphere with respect to the observer, with contributions from thermal motions, winds and, particularly, acoustic waves. The situation is nicely defined by Young [1981]: "To summarize: molecular scattering consists of Rayleigh scattering and vibrational Raman scattering. The Rayleigh scattering consists of rotational Raman lines and the

central Cabannes line. The Cabannes line is composed of the Brillouin doublet and the central Gross or Landau-Placzek line. None of the above is completely coherent. The term 'Rayleigh line' should never be used." Note that the vibrational Raman contribution results in lines so widely separated from the frequency of the incoming light that they are not normally considered part of the "Ring effect" even though in recent applications the Ring effect has developed a somewhat broader definition that includes substantial interfering structure in observations, rather than the initial effect which was limited to broadening of partially-resolved lines.

The Ring effect has become more important in recent years with the increase in ultraviolet and visible spectroscopic observations of the Earth's atmosphere from the ground [Solomon *et al.*, 1987; Fish and Jones, 1995] and from satellites [Chance *et al.*, 1991a; Burrows *et al.*, 1993; Joiner *et al.*, 1995; Joiner and Bhartia, 1995]. In order to retrieve abundances of trace species from many such observations it is necessary to take the Ring effect into account. Methods have been developed to do so by pragmatic means, by measuring the polarization of scattered sunlight [Solomon *et al.*, 1987] and by modeling of the effect directly from molecular scattering processes [Fish and Jones, 1995; Joiner *et al.*, 1995]. It has been proposed to use the Ring effect with selected Fraunhofer lines (in particular, the CaI h and k lines) to determine cloud parameters in conjunction with satellite-based observations of O₃ [Joiner and Bhartia, 1995]. Joiner *et al.* [1995] also determined that the contribution to the Ring effect from the Rayleigh-Brillouin scattering process is negligible for most geometries used in satellite observations. For the European Space Agency's Global Ozone Monitoring Experiment (GOME) and the upcoming Scanning Imaging Absorption Spectrometer for Atmospheric Chartography (SCIAMACHY), as well as proposed future space-based

atmospheric monitoring which emphasize tropospheric measurements, the use of visible bands of O₂, in particular the 762 nm A band, for determination of cloud parameters is being developed [Kuze and Chance, 1994]. The Ring effect has a substantial influence on such observations and work is underway in our institution to refine and model the effects. In this case, the effect is due to inelastic scattering in molecular absorption lines themselves, rather than in the solar Fraunhofer lines. Similar effects have been noted for the detailed retrieval of trace species including O₃ and NO₂ [Solomon *et al.*, 1987; Fish and Jones, 1995; J.P. Burrows, private communication, 1995].

The present work is part of an ongoing effort to quantify the Ring effect for atmospheric radiative transfer modeling, with application to satellite- and ground-based measurements, and to apply it to particular cases such as the detailed absorption in the O₂ bands. Much of previous modeling work has relied on the development of molecular parameters for N₂ and O₂ by Penney *et al.* [1974] (e.g., Bussemer [1993], Fish and Jones [1995]; Joiner *et al.* [1995]) with one study updating the dynamic polarizability anisotropies as developed by Bates [1994] (Joiner *et al.* [1995]). Previous work has largely ignored the complication of the rotational Raman spectrum of O₂ caused by the electronic spin angular momentum in the ³Σ_g⁻ ground state and the issue of pressure broadening of the rotation Raman lines. In this publication we update the molecular parameters and the scattering with respect to the solar Fraunhofer spectrum using the best currently available laboratory and field data and theoretical studies of which we are aware. This provides: An updated expression for Rayleigh scattering by air; expressions for the wavelength-dependent polarizability anisotropies of O₂ and N₂; accurate Placzek-Teller coefficients (the state-dependent factors in the line intensities) for O₂ rotational Raman lines; a tentative set of pressure broadening coefficients for the O₂ and N₂ rotational Raman lines; A solar reference spectrum for convolution with calculated Ring cross sections; and a convolved Fraunhofer-rotational Raman source spectrum for fitting of atmospheric spectra. The tables and spectra are not included here due to size limitations. They are available from the authors.

2. RAYLEIGH SCATTERING

To examine the detailed Rayleigh and rotational Raman scattering properties, including their rela-

tive intensities and the scattering phase functions, we begin with Table I of Kattawar *et al.* [1981]. This table describes the relative intensities and angular behavior for the Rayleigh-Brillouin and rotational components, and their sum, for various input polarizations, including unpolarized light (the predominant contribution for most atmospheric observations where single scattering is the major contributor to the Ring effect). For unpolarized light the depolarization ratios (defined in each case as the ratio of the horizontally-polarized component to the vertically-polarized component at 90° scattering angle) may be determined directly. Table I of Kattawar *et al.* [1981] is reproduced here as Table 1, with the addition of the depolarization ratios, for the three cases: Rayleigh-Brillouin (the central Cabannes component, *C*); rotational Raman (the wings, *W*); and the sum of the two (*R*, for Rayleigh). The phase functions for scattering may also be derived for each case. They are given here normalized over solid angle to 1.

$$\begin{aligned}\Phi_0^C &= \frac{3}{160\pi} \left[\frac{(180 + 13\epsilon) + (180 + \epsilon) \cos^2\theta}{18 + \epsilon} \right] \\ \Phi_0^W &= \frac{3}{160\pi} (13 + \cos^2\theta) \\ \Phi_0^R &= \frac{3}{80\pi} \left[\frac{(45 + 13\epsilon) + (45 + \epsilon) \cos^2\theta}{9 + 2\epsilon} \right]\end{aligned}\quad (1)$$

In each case, the phase function is given in terms of the *respective* depolarization ratio ($X = C, W, R$)

$$\Phi_0^X = \frac{3}{8\pi} \left[\frac{(1 + \rho_0^X) + (1 - \rho_0^X) \cos^2\theta}{2 + \rho_0^X} \right]. \quad (2)$$

The Rayleigh scattering cross section at standard temperature (273.15 K) and pressure (1 atmosphere) is given by

$$Q_R = \frac{32\pi^3(n-1)^2 F_K}{3N_0^2 \lambda^4} \quad (3)$$

where n is the index of refraction, F_K is the King correction factor (King [1923]), N_0 is Loschmidt's number ($2.686763 \times 10^{19} \text{ cm}^{-3}$), and λ is the wavelength. The King correction factor is given by

$$F_K = 1 + 2 \left(\frac{\gamma}{3\bar{\alpha}} \right)^2 = \frac{6 + 3\rho_0^R}{6 - 7\rho_0^R} \quad (4)$$

where γ is the anisotropy of the polarizability and $\bar{\alpha}$ is the average polarizability. The average polarizability can be determined from

$$|\bar{\alpha}|^2 = \frac{(n-1)^2}{4\pi^2 N_0^2}. \quad (5)$$

3. MOLECULAR PARAMETERS

3.1 Rayleigh scattering cross sections

The major source of improved data for the index of refraction of air (and of O₂ and N₂) versus wavelength, the King correction factors, and the anisotropies of the polarizabilities) is Bates [1984]. He presents a comprehensive review of both measurements and theoretical calculations to derive a data set that is demonstrated to be better than 1% for all data and parameterizations presented here.

Bates' [1984] Table 1 gives refractive indices, Rayleigh scattering cross sections, and King correction factors versus wavelength for air from 200-1000 nm. The index of refraction data are fitted here to an Edlén-type expression to better than 0.1% for all values:

$$(n_{air} - 1) \times 10^4 = 0.7041 + \frac{315.90}{157.39 - \sigma^2} + \frac{8.4127}{50.429 - \sigma^2} \quad (6)$$

where σ (μm^{-1}) = $1/\lambda$ (μm). The Rayleigh cross sections are reproduced to better than 1% by the expression

$$Q_R \times 10^{24} (\text{cm}^2) = \frac{3.9993 \times 10^{-4} \sigma^4}{1 - 1.069 \times 10^{-2} \sigma^2 - 6.681 \times 10^{-5} \sigma^4} \quad (7)$$

The King factor and depolarization for any choice of wavelength within the 0.2-1.0 μm range can be accurately determined from the previous two equations.

3.2 Polarizability anisotropies

The previous expansions are for air, including standard amounts of Ar and CO₂. For rotational Raman cross sections we will limit the calculations to O₂ and N₂. Bates gives segmented representations for the indices of refraction of O₂ and N₂ versus wavelength and expansions for the respective King correction factors. Tables giving the King correction factors, values of $\sqrt{\epsilon}$, where $\epsilon = (\gamma/\bar{\alpha})^2$, index of refraction $\bar{\alpha}$, and γ for O₂ and N₂ are available from the authors. From these data γ_{O_2} is determined to better than 1% over this wavelength range by

$$\gamma_{O_2} \times 10^{24} = 0.07149 + \frac{45.9364}{48.2716 - \sigma^2} \quad (8)$$

and γ_{N_2} to much better than 1% by

$$\gamma_{N_2} \times 10^{25} = -6.01466 + \frac{2385.57}{186.099 - \sigma^2} \quad (9)$$

These equations should be considered merely as phenomenological fits over the particular wavelength range, rather than trying to attach physical importance to (for example) the negative value of the constant term in the N₂ equation. Extrapolation to outside the 0.2 - 1.0 μm range should be considered perilous.

3.3 Basic spectroscopy

The ground state of O₂ is $^3\Sigma_g^-$; it has significant electronic structure in both its magnetic dipole rotational and rotational Raman spectra. Rotational Raman spectra of both O₂ and N₂ have previously been approximated by simple expansions in the lowest rotational parameters (for positions) and by using T/c_2B_0 for the rotational partition functions. Very precise data are now available for the term energies, allowing line positions and Boltzmann factors to be accurately and rapidly calculated. The use of term values from the current HITRAN listing [Rothman *et al.*, 1992] allows for calculations of lines positions to 0.0001 cm^{-1} accuracy and highly accurate statistical partitioning. Tables including the quantum numbers and term energies for O₂ and N₂ up to states allowing for partitioning to better than 0.01% accuracy and Boltzmann factors (with nuclear spin degeneracies, g_N) are available from the authors.

3.4 Placzek-Teller coefficients

Cross sections for rotational Raman scattering are given by

$$Q_{N,N'}^W (\text{cm}^2) = \frac{256\pi^5}{27(\lambda')^4} \gamma^2 f_N c_{PT}(N, J, N', J'), \quad (10)$$

where f_N is the fractional population in the initial state. The quantum state-dependent factors $c_{PT}(N, J, N', J')$ are commonly known as "Placzek-Teller coefficients" from the initial derivations [Placzek and Teller, 1933]. These factors are given for a molecule in a Σ electronic state with one electronic spin angular momentum, in a Hund's case b coupling scheme (electron spin coupled to rotational angular momentum), by

$$c_{PT}(N, J, N', J') = (2N+1)(2N'+1)(2J'+1) \times \begin{pmatrix} N & L & N' \\ 0 & 0 & 0 \end{pmatrix}^2 \left\{ \begin{matrix} N & L & N' \\ J' & S & J \end{matrix} \right\}^2 \quad (11)$$

where J is the total angular momentum, S is the electronic spin angular momentum (1 for O₂ and 0 for N₂), and L is the component of the 2nd rank

polarizability tensor. $L = 0$ for average polarizability (The Cabannes component) and $L = 2$ for the present Raman scattering. The standard definitions for 3- j and 6- j coefficients are used. Near equivalents to this equation are given in Renschler *et al.* [1969] and in Loëte and Berger [1977] (both give the formula for "line strengths" which include the initial state degeneracy). For $S = 0$ (*i.e.*, N_2), eq. 11 reduces to the result of Penney *et al.* [1974], eq. 7:

$$\begin{aligned} c_{PT}(J \rightarrow J+2) &= \frac{3(J+1)(J+2)}{2(2J+1)(2J+3)} \quad (12) \\ c_{PT}(J \rightarrow J) &= \frac{J(J+1)}{(2J-1)(2J+3)} \\ c_{PT}(J \rightarrow J-2) &= \frac{3J(J-1)}{2(2J+1)(2J-1)}. \end{aligned}$$

This derivation gives correct Placzek-Teller coefficients for N_2 , but approximates those for O_2 by treating it as a pure Hund's case b molecule. At low N, J the departures from the pure coupling case due to the electron spin-rotation interaction are enough to significantly affect the spectrum, as noted by Renschler *et al.* [1969] and Rich and Lepard [1971]. In the classic study of the O_2 ground state, Tinkham and Strandberg [1955] include the correct eigenvectors for levels up to $J = 26$ in the case b basis set (their Table V and equation 54). Above this level the molecule is described by case b behavior to a very high degree of accuracy. For $J = 0$ and all odd J levels the case b description is exact. For even J levels, $J \neq 0$, the transformation from case b basis functions $\phi_{N,J}$ to eigenfunctions $\Psi_{N,J}$ is given by

$$\begin{aligned} \Psi_{J-1,J} &= b_J \phi_{J-1,J} - d_J \phi_{J+1,J} \quad (13) \\ \Psi_{J+1,J} &= d_J \phi_{J-1,J} + b_J \phi_{J+1,J}. \end{aligned}$$

The b_J and d_J values from Tinkham and Strandberg [1955] are used here to calculate correct Placzek-Teller coefficients for values up to $J = 10$, above which the corrections become completely negligible. The database calculated using the corrected eigenvectors is prepared with an intensity cutoff to include all rotational Raman lines with intensities at 296 K within 0.1% of the strongest line. Because of the mixing of states, this now includes two $\Delta N = 4$ transitions. An almost identical result was determined by Altmann *et al.* [1972] who calculated eigenvectors for the secular determinant and molecular parameters given in the slightly earlier work of Mizushima and Hill [1954].

3.5 Pressure broadening coefficients

Γ is used here for the full-width at half-maximum pressure broadening coefficient to distinguish it from the γ used for anisotropy of polarizability. The best existing measurements of pressure broadening for the rotational Raman lines are from Jammu *et al.* [1966]. These authors note some evidence that the unresolved Q branches of vibrational Raman bands seem to broaden less than lines due to ordinary dipole transitions, but that the rotational Raman lines broaden comparably to dipole transitions. They present self-broadening measurements for N_2 , O_2 , CO_2 , and CO , as well as He and Ar broadening of N_2 , O_2 . All measurements were made at room temperature. Given the experimental conditions (very high pressures, modest spectral resolution) and the lack of air-broadening measurements, temperature dependences, and a tabulation of the J -dependent N_2 broadening coefficients, it was decided not to use these measurements as the basis for broadening in the present data set. Instead, for O_2 the HITRAN92 values corresponding to rotational transitions of the same ΔN are initially adopted [Rothman *et al.*, 1992]. Where multiple corresponding transitions exist, the pressure broadening coefficients are averaged. For the two $\Delta N = 4$ transitions, the average of the values for lines connecting the upper and lower states is taken. The resulting pressure broadening coefficients are multiplied by 1.185, which is the average result for the ratio of measured air pressure broadening coefficients for O_2 magnetic dipole rotational transitions to those given in HITRAN (see Chance *et al.* [1991b] for an explanation of this correction). For N_2 , pressure broadening values for the corresponding quadrupole lines of the vibrational fundamental are adopted. Values listed for the pressure broadening coefficients of both O_2 and N_2 are at 296 K. The temperature dependence should be calculated using the recommended HITRAN92 coefficient of $n = 0.5$ for N_2 lines [Rothman *et al.*, 1992] and a value of $n = 0.72$ for O_2 lines [Chance *et al.*, 1991b], where

$$\Gamma_T = \Gamma_{296} \times \left(\frac{296}{T} \right)^n. \quad (14)$$

4. SOLAR REFERENCE AND RING SOURCE SPECTRA

A solar reference spectrum for the range 230-800 nm, at 0.01 nm resolution has been determined by combining ground-based measurements [Kurucz *et al.*, 1984] and balloon measurements [Hall and Anderson, 1991] and re-calibrating in wavelength. The

spectrum is given at 0.01 nm resolution, in vacuum wavelengths accurate to better than 0.001 nm above 305 nm and 0.002 nm below 300 nm. It will be described more fully in a future publication. The purposes for constructing such a spectrum include GOME wavelength calibration studies and calculating Ring effect contributions to GOME measurements. The solar spectrum has been convolved with the rotational Raman cross sections described here to create a source spectrum for fitting of GOME data. The solar spectrum and solar-rotational Raman convolved spectra, with and without the GOME slit function, are available from the authors.

5. CONCLUSIONS

The complete rotational Raman scattering database as described in the previous sections is available from the authors. This is a summary of the best available data that were found in the present investigation, and subsequent calculations. It provides a substantial improvement in the ability to model the atmospheric Ring spectrum, particularly when it is combined with the updated values of the wavelength dependent polarizability anisotropies also included in this study. One item not included here is the additional broadening due to Rayleigh-Brillouin scattering [Kattawar *et al.*, 1981]. For the rotational Raman lines, this will provide an extra source of broadening, although the extent of the broadening is within the uncertainties in the pressure broadening for scattering in the troposphere. The effect of Rayleigh-Brillouin scattering for the filling in of the central Cabannes line for narrow Fraunhofer lines might be significant for some satellite measurement conditions, although it has been found to be negligible for SBUV measurements [Joiner *et al.*, 1995]. During the course of the study, several references relating to vibrational Raman scattering were uncovered. These are included in the references with appropriate notation.

6. REFERENCES

K. Altmann, G. Strey, J.G. Hochenbleicher, and J. Brandmüller, Simulation des intensitätsverlaufs im Raman-spektrum von sauerstoff unter berücksichtigung der spinaufspaltung, *Z. Naturforsch.* **27a**, 56-64, 1972.

D.R. Bates, Rayleigh scattering by air, *Planet. Space Sci.* **32**, 785-790, 1984.

J.P. Burrows, K.V. Chance, A.P.H. Goede, R.

Guzzi, B.J. Kerridge, C. Muller, D. Perner, U. Platt, J.-P. Pommereau, W. Schneider, R.J. Spurr, and H. van der Woerd, *Global Ozone Monitoring Experiment Interim Science Report*, ed. T. D. Guyenne and C. Readings, Report ESA SP-1151, ESA Publications Division, ESTEC, Noordwijk, The Netherlands, ISBN 92-9092-041-6, 1993.

M. Bussemer, Der Ring-effekt: Ursachen und einfluß auf die spektroskopische messung stratosphärischer spurenstoffe, Diplomarbeit, Universität Heidelberg, 1993.

K.V. Chance, J.P. Burrows, and W. Schneider, Retrieval and molecule sensitivity studies for the Global Ozone Monitoring Experiment and the SCanning Imaging Absorption spectroMeter for Atmospheric CHartographY, *Proc. S.P.I.E., Remote Sensing of Atmospheric Chemistry*, **1491**, 151-165, 1991a.

K. V. Chance, W. A. Traub, K. W. Jucks, and D. G. Johnson, On the use of O₂ spin-rotation lines for elevation angle calibration of atmospheric thermal emission spectra, *Int. J. IR-MM Waves* **12**, 581-588, 1991b.

D.J. Fish and R.L. Jones, Rotational Raman scattering and the Ring effect in zenith-sky spectra, *Geophys. Res. Lett.* **22**, 811-814, 1995.

J.F. Grainger and J. Ring, Anomalous Fraunhofer line profiles, *Nature* **193**, 762, 1962.

L.A. Hall and G.P. Anderson, High-resolution solar spectrum between 200 and 3100 Å, *J. Geophys. Res.* **96**, 12,927-12,931, 1991.

D.M. Hunten, Surface albedo and the filling-in of Fraunhofer lines in the day sky, *Astrophys. J.* **159**, 1107-1110, 1970.

K.S. Jammu, G.E. St. John, and H.L. Welsh, Pressure broadening of the rotational Raman lines of some simple gases, *Can. J. Phys.* **44**, 797-815, 1966.

J. Joiner, P.K. Bhartia, R.P. Cebula, E. Hilsenrath, R.D. McPeters, and H. Park, Rotational Raman scattering (Ring effect) in satellite backscatter ultraviolet measurements, *Appl. Opt.* **34**, 4513-4525, 1995.

J. Joiner and P.K. Bhartia, The determination of cloud pressures from rotational Raman scattering in satellite backscatter ultraviolet measurements, *J. Geophys. Res.* **100**, 23,019-23,026, 1995.

G.W. Kattawar, A.T. Young, and T.J. Humphreys,

Inelastic scattering in planetary atmospheres. I. The Ring effect, without aerosols, *Astrophys. J.* **243**, 1049-1057, 1981.

L.V. King, On the complex anisotropic molecule in relation to the dispersion and scattering of light, *Proc. Roy. Soc. A* **104**, 333-357, 1923.

R.L. Kurucz, I. Furenlid, J. Brault, and L. Testerman, Solar Flux Atlas from 296 to 1300 nm, National Solar Observatory, Sunspot, New Mexico, 240 pp., 1984.

A. Kuze and K. V. Chance, Analysis of cloud-top height and cloud coverage from satellites using the O₂ A and B bands, *J. Geophys. Res.* **99**, 14,481-14,491, 1994.

M. Loëte and H. Berger, High resolution Raman spectroscopy of the fundamental vibrational band of ¹⁶O₂, *J. Molec. Spectrosc.* **68**, 317-325, 1977.

M. Mizushima and R.M. Hill, Microwave spectrum of O₂, *Phys. Rev.* **93**, 745-748, 1954.

J. Noxon and R. Goody, Noncoherent scattering of skylight, *Izv. Atmos. Ocean. Phys.* **1**, 163-166, 1965.

C.M. Penney, R.L. St. Peters, and M. Lapp, Absolute rotational Raman cross sections for N₂, O₂,

and CO₂, *J. Opt. Soc. Amer.* **64**, 712-716, 1974.

G. Placzek and E. Teller, Die rotationstruktur der Ramanbanden mehratomiger molekule, *Z. Physik* **81**, 209-258, 1933.

D.L. Renschler, J.L. Hunt, T.K. McCubbin, Jr., and S.R. Polo, Triplet structure of the rotational Raman spectrum of oxygen, *J. Molec. Spectrosc.* **31**, 173-176, 1969.

N.H. Rich and D.W. Lepard, Spin structure in the Raman spectrum of oxygen, *J. Molec. Spectrosc.* **38**, 549-551, 1971.

S. Solomon, A.L. Schmeltekopf, and R.W. Sanders, On the interpretation of zenith sky absorption measurements, *J. Geophys. Res.* **92**, 8311-8319, 1987.

M. Tinkham and M.W.P. Strandberg, Theory of the fine structure of the molecular oxygen ground state, *Phys. Rev.* **97**, 937-951, 1955.

A.T. Young, Rayleigh scattering, *Appl. Opt.* **20**, 522-535, 1981.

7. ACKNOWLEDGEMENTS

This research was supported by NASA grant NAGW-2541 and by ESA contract 10996/94/NL/CN.

TABLE 1. Relative Rayleigh and Raman Scattering Intensities
Mostly from Kattawar *et al.*, 1981

V polarization in	H polarization in	Sum (natural light in)
Rayleigh-Brillouin		
${}^V C_V = 180 + 4\epsilon$	${}^H C_V = 3\epsilon$	${}^0 C_V = 180 + 7\epsilon$
${}^V C_H = 3\epsilon$	${}^H C_H = 3\epsilon + (180 + \epsilon) \cos^2\theta$	${}^0 C_H = 6\epsilon + (180 + \epsilon) \cos^2\theta$
${}^V C_0 = 180 + 7\epsilon$	${}^H C_0 = 6\epsilon + (180 + \epsilon) \cos^2\theta$	${}^0 C_0 = (180 + 13\epsilon) + (180 + \epsilon) \cos^2\theta$
		$\rho_0^C = 6\epsilon/(180 + 7\epsilon)$
Raman		
${}^V W_V = 12\epsilon$	${}^H W_V = 9\epsilon$	${}^0 W_V = 21\epsilon$
${}^V W_H = 9\epsilon$	${}^H W_H = 9\epsilon + 3\epsilon \cos^2\theta$	${}^0 W_H = 18\epsilon + 3\epsilon \cos^2\theta$
${}^V W_0 = 21\epsilon$	${}^H W_0 = 18\epsilon + 3\epsilon \cos^2\theta$	${}^0 W_0 = 39\epsilon + 3\epsilon \cos^2\theta$
		$\rho_0^W = 6/7$
Sum		
${}^V T_V = 180 + 16\epsilon$	${}^H T_V = 12\epsilon$	${}^0 T_V = 180 + 28\epsilon$
${}^V T_H = 12\epsilon$	${}^H T_H = 12\epsilon + (180 + 4\epsilon) \cos^2\theta$	${}^0 T_H = 24\epsilon + (180 + 4\epsilon) \cos^2\theta$
${}^V T_0 = 180 + 28\epsilon$	${}^H T_0 = 24\epsilon + (180 + 4\epsilon) \cos^2\theta$	${}^0 T_0 = (180 + 52\epsilon) + (180 + 4\epsilon) \cos^2\theta$
		$\rho_0^T = 6\epsilon/(45 + 7\epsilon)$

53-46

98143

246192

close

GOME Calibration and Validation Using Backscatter UV Techniques 8P.

E. Hilsenrath¹, J. Gleason¹, S. Janz², X-y Gu³, R.P. Cebula³, K. Chance⁴, and R. Hoekstra⁵

1. NASA/Goddard Space Flight Center
2. IDEA Corporation
3. Hughes-STX Corporation
4. Smithsonian Astrophysical Society
5. TNO/TPD

Abstract

GOME radiance, irradiance, and ozone products were validated by NASA, Goddard Space Flight Center through three tasks which included, pre-launch calibration comparisons with SBUV and TOMS radiometric standards, validation of GOME Level-1 irradiance and radiance and Level 2 total ozone data products using SBUV/2 and TOMS algorithms and data, and studies of GOME data using the Goddard radiative transfer code. The pre-launch calibration using the NASA large aperture integrating sphere was checked against that provided by TPD. Agreement in the calibration constants, derived in air, between the Goddard and TPD system were better than 3%. Validation of Level-1 irradiance data included comparison of GOME and SSBUV and the UARS solar irradiances measurements. Large wavelength dependent differences, as high as 10%, were noted between GOME and the US instruments. This discrepancy has now been attributed to radiometric sensitivity changes experienced by GOME when operating in a vacuum. GOME Earth radiance data were then compared to the NOAA-14 SBUV/2 radiances. These results show that between 340 and 400 nm the differences in GOME and SBUV/2 data are less than 5% with some wavelength dependence. At wavelengths shorter than 300 nm, differences are of the order of 10% or more where the GOME radiances are larger. To test GOME DOAS retrieved total ozone values, these values were compared with ozone amounts retrieved using GOME radiances in the TOMS version-7 algorithm. The differences showed a solar zenith angle dependence ranging from 0 to 10% where the TOMS algorithm values were higher. GOME radiances below 300 nm were further validated by selecting radiances at wavelengths normally used by SBUV and processing them through the SBUV ozone profile algorithm and then compared to climatological values. The GOME ozone profiles ranged from 10-30% lower over altitude compared to climatological values. This is consistent with the offsets detected in the SBUV/2 radiance comparisons at wavelengths shorter than 300 nm.

Introduction

NASA Goddard Space Flight Center has participated in the GOME validation through an ESA announcement of opportunity. The proposed validation investigation included three tasks: 1) Pre-launch calibration evaluation, 2) Post launch data validation, and 3) Algorithm studies using GOME data. The validation effort focused primarily on GOME data from Channels 1 and 2. These channels

cover the wavelength range 240 to 405 nm which overlap wavelengths covered by NASA's SBUV and TOMS instruments. Our overall goal is to develop a consistent, long term, global ozone data set through better understanding of instrument performance and radiative transfer properties of the atmosphere. A description of the methodology for pre- and post-launch calibration, validation, and of producing long term data sets from US SBUV instruments has been reviewed by *Hilsenrath et al.*, 1994.

In this progress report we describe briefly results from the pre-launch calibration activity using NASA calibration standards, post-launch validation of Level 1 irradiances and radiances from comparisons with SSBUV and NOAA-14 SBUV/2 modeled radiances and Level 2 DOAS ozone retrievals compared with SBUV ozone retrievals using the Level 1 GOME radiance in the TOMS version 7 and SBUV profile algorithms. Finally we have conducted very preliminary algorithm research using GOME radiance to study the Ring effect and the effect of absorbing aerosols on the GOME radiances. The GOME Level 1 and Level 2 data used in this first phase of validation was received from the DLR up until December, 1996 on CD-ROMs.

1. Pre-launch Calibration Intercomparison

Backscatter measuring instruments such as TOMS, SBUV, and GOME require careful calibrations to determine sensitivity to both Earth radiance and the Solar irradiance. Irradiance calibrations are derived by illuminating the instrument with an irradiance standard provided by a national laboratory such as the US National Institutes for Standards and Technology. However, there are no standards for radiance applicable for remote sensors with extended fields of view, therefore flat diffuser plates illuminated by an irradiance source are used as a radiance target. Traditional flat plate calibrations have been subject to large uncertainties due to the difficulty in the measurement of the angular distribution of the diffuse scattering from the targets. Inconsistencies in bidirectional reflectance distribution function (BRDF) measurements on the order of 10% were not uncommon in the past [*Heath, et al.*, 1993]. The sphere based calibration technique was

developed to enhance the accuracy of extended source radiance based calibrations, and to provide a baseline for the continuing improvement in BRDF measurements. The sphere technique is inherently less prone to systematic errors due to the simplicity of the calibration set-up, and requires only that one can measure accurately the sphere port area and the distance to the target. Additionally, the sphere is easily transportable allowing for on-site inter-calibrations to be performed. Recent results from comparisons of this technique with flat plate calibrations on the SSBUV, TOMS, and SBUV/2 yield agreement on the 2-3 % level. [Janz *et al.*, 1996].

Calibration of GOME has been reviewed by Hahne *et al.*, [1994]. The cross-calibration of SSBUV with both the GOME FSM and FM instruments using NASA's integrating sphere as a transfer was performed at TPD in the fall of 1994, [Heath *et al.*, 1994]. The results indicated very good consistency (2-3 % level) between the sphere based radiance sensitivity and the flat plate based sensitivity over the wavelength range that the sphere was calibrated, 250 nm - 450 nm. There was also good consistency between flat plate techniques using targets measured both by TPD and the Goddard BRDF facility. The good agreement among the various calibration techniques and set-ups provides a large degree of confidence that the GOME instrument and SSBUV are on a common radiometric scale, traceable to NIST standards, and provide a solid baseline for inter-comparisons of these instruments while in space. Further details of the ground calibration are reported elsewhere in this volume.

2. Post-launch Validation of Level 1 Data

Plans for Level-1 validation of GOME included comparison of GOME solar irradiance and Earth radiance data with the TOMS, SBUV/2, and SSBUV. The eighth flight of SSBUV was conducted in January 1996 for which there are no GOME data yet available. The Earth Probe TOMS launch has been postponed until mid 1996. The SBUV/2 on NOAA-14 was launched in December, 1995 but has only recently become operational because of numerous spacecraft and instrument problems. Therefore, Level 1 radiance comparisons has been limited to a few number of comparisons using specially processed data for this validation effort. GOME solar irradiances have been compared to earlier SSBUV flights as well as the UARS instruments. The detailed UARS comparisons, particularly the SOLSTICE is being reported elsewhere in this volume however comparisons with SSBUV are summarized below.

Solar irradiance

GOME solar irradiance comparisons with SSBUV and the UARS SOLSTICE and SUSIM instruments show

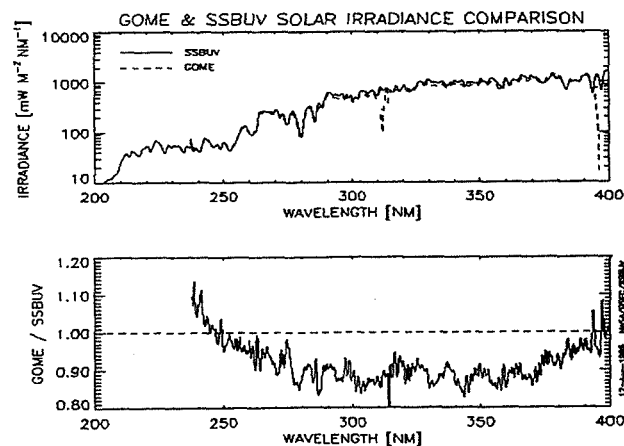


Figure 1. GOME SSBUV Solar irradiance comparison

significant differences (10-20%) particularly at wavelengths between 260 and 290 nm. A comparison with SSBUV data is shown in Figure 1 and is very similar to the comparisons of GOME and the UARS instruments. Comparisons among the US solar irradiances show agreement to better than 3% over wavelength with nearly zero systematic differences (Woods *et al.*, 1996, Cebula, *et al.*, 1996). Therefore the difference seen in figure 1 are primarily due to errors in GOME. These differences have now been explained to result from air-to-vacuum changes in GOME sensitivity. Similar changes have been observed in SBUV/2 instruments and are attributed to out-gassing from protective coating used on the GOME instrument's optical surfaces. ESA, TPD, and the University of Bremen are developing correction a factor to account for this sensitivity change. As GOME irradiances are refined additional comparisons will be made with the SSBUV-8, the UARS instruments and SBUV/2 on NOAA-14

Earth Radiances Comparisons

Comparisons of GOME radiances with SBUV/2, TOMS, and SSBUV have been limited for reasons mentioned above. To enhance the validation with limited data, a radiative transfer model was developed to compute radiance from SBUV/2 ozone data anywhere in the vicinity of a GOME observation. The model is particularly useful since SBUV observations are only made at 12 discrete channels with 1.1 nm resolution. Therefore the model affords a comparison over all wavelengths at the GOME wavelength resolution. In addition, special NOAA-14 SBUV/2 and GOME data sets were compiled for the period August 25-27 over Mauna Loa, Hawaii during a Network for Detection of Stratospheric Change (NDSC) ground based ozone intercomparison campaign. This campaign provided independently validated total ozone and profile ozone data from NOAA-14 using

SBUV/2 data over Hawaii.

The model to calculate radiances applicable to GOME channels 1 and 2 radiances involves the Dave-Mateer radiative transfer code [Dave, 1964], which is the major tool in the BUV processing and analysis. The Earth's backscattered radiance is a function of the solar zenith angle, the ozone profile shape and the surface reflectivity which all have to be accounted for in model calculation. The model has recently been updated to include Raman Scattering (Ring effect) [Joiner et al., 1995]. To model the GOME radiances for a given ground pixel, the GOME measured radiance at 380 nm is used for derivation of the surface reflectivity and includes the solar zenith angle at the GOME measurement. From these parameters the theoretical radiance, which is the sum of the single scattered (SS) and the multiple scattered and reflected (MSR) radiances, are computed. For radiance calculations shorter than 340 nm the ozone profile measured independently, e.g. SBUV/2, is included to compute the theoretical radiances. The MSR component depends primarily on the total column ozone and the surface reflectivity. For practical applications of the model and GOME comparisons, the normalized radiances (the ratio of the Earth radiance to solar irradiance which is proportional to the directional albedo, (hereinafter simply called 'radiances')) are employed.

Based on these principals, the GOME radiances are calculated using Bass and Paur cross sections at about 0.05 nm steps. As the last step in the calculation of the GOME radiances, an integration is implemented to take into account the GOME slit width, including the GOME slit function in its integrand. Since the integration needs to be computed in wavelength (λ) space, a partial derivative of λ with respect to the pixel number p was applied to convert Δp into $\Delta \lambda$ in the form of the GOME slit function.

The GOME measured and the theoretical values are then compared by analyzing the percent differences between the measured GOME radiances with the theoretically computed radiances. This difference is called the residue. This method was successfully applied to the SBUV continuous scan data in revealing spectral anomalies in the data and validation of Dave-Mateer radiative transfer code [Gu et al., 1996]. In order to minimize impact from ozone profile errors, a non-ozone absorbing wavelength range of 340 - 400 nm was first chosen for this comparison.

Figure 2 shows the residue described above and the residue due to the Ring effect. The Ring effect residue is calculated from the GOME measured solar irradiance, the solar zenith angle, and the surface pressure [Joiner et al., 1995]. For this case the reflectivity was low therefore a near ground pressure was assumed. For this analysis, 22 GOME nadir ground pixels over the Arabian Sea on July

23 were used. The solar zenith angles were large enough

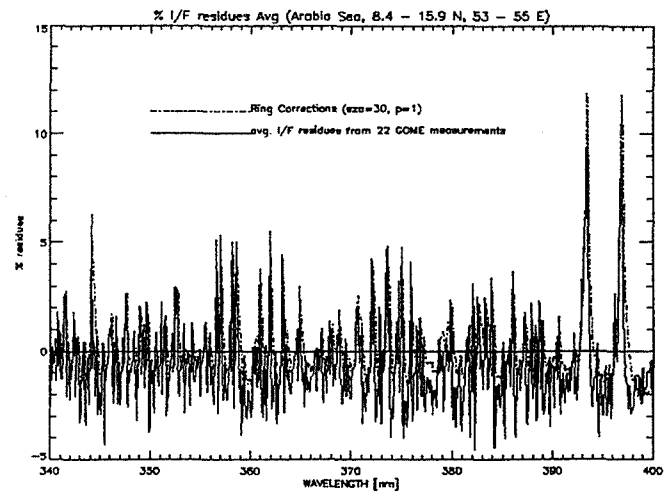


Figure 2. Residue comparing GOME and calculated radiance. Ring effect residues are also shown.

(>25°) so that sea glint is not a concern but were also small enough (<30°) that the polarization corrections are not important. On average the residues are small meaning that the GOME calibration is accurate to the order of 1% where the unaccounted for Ring effect amounts to a peak-to-peak "noise" of about 5%. Close inspection of the two curves in Figure 2 reveals a systematic wavelength misalignment of about 0.06 nm. Studies of SBUV continuous scan data, demonstrated that a small wavelength shift ($d\lambda$) between the earth radiance (I) and solar irradiance (F) may generate about ten times larger wavelength shift $\Delta \lambda$ in the normalized radiances. For example, the observed 0.06 nm misalignment might be generated by $d\lambda$ of 0.006 nm, which is smaller than the GOME tolerance of 0.0156 nm. To further refine the comparison, two additional steps were taken. The first was to account for the Ring effect and the second to adjust the wavelength to match the location of the Fraunhofer lines. Figure 3 indicates that after these adjustments the 'final' residue is about $\pm 1\%$ peak-to-peak with an offset or calibration error of about 1%. These results are comparable to the findings using SBUV data. Work has begun to further understand the remaining structure in the 'final' residues.

Additional residues from other geographical locations were also analyzed to understand GOME radiances compared to the model calculations. Figure 4 illustrates the 'final' (wavelength adjusted and Ring effect removed) residues for other samples of selected nadir ground pixel over the Sahara desert in August. Comparing this figure to Figure 3, several differences are seen. These features could be due to several factors such as, residual Ring

effect, aerosol scattering, key data, or calibration errors.

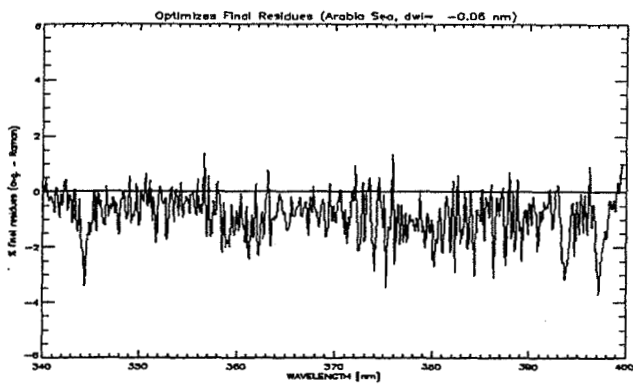


Figure 3. Final residue includes wavelength adjustment and removal of Ring effect.

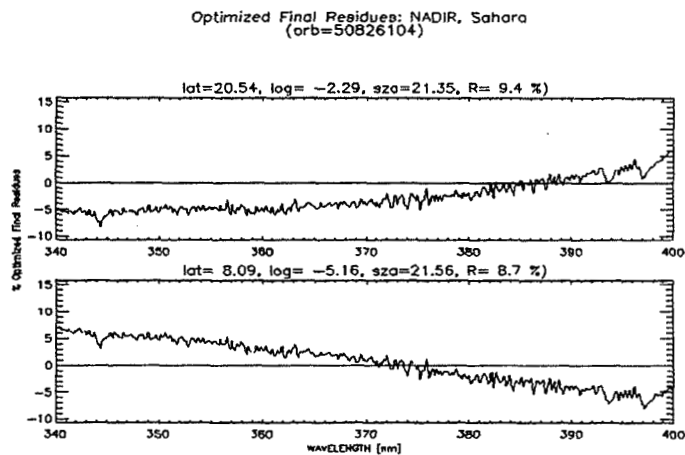


Figure 4. Final residue over Sahara desert in August.

Recent investigation of TOMS data [Hsu et al., 1996] have shown reflectivity anomalies (among only two wavelengths) which could be associated with smoke and dust. These anomalies result from absorbing aerosols which cause a wavelength dependent signature in the residues. The upper curves in Figure 4 represents a 'final' residue with a clear sky (reflectivity of 9%). The polarization corrections are extremely small because of the surface property and low SZA (about 20°). Figure 4 shows both a positive (upper curve) and negative (lower curve) reflectivity anomaly with respect to wavelength. The lower curve reflects what is seen in TOMS data and our radiative transfer model (Torres and Bhartia, 1995) which is associated with desert dust. This is by no means a definitive study of GOME observations of the spectral signatures of absorbing aerosols. Studies of GOME data are planned with comparison to the 12 year record of TOMS data.

In order to validate GOME radiances from 250 nm to 400 nm, radiances were calculated from a special processing of NOAA-14 SBUV/2 data taken over Mauna Loa, Hawaii during an NDSC ozone intercomparison campaign conducted in August 1995. This intercomparison campaign provides an excellent opportunity to validate the SBUV/2 data used to compare with the GOME data. Figure 5 illustrates the comparability of the SBUV/2 with several ground based lidar and microwave measurements as well as Umkehr and balloon soundings for August 25, 1995.

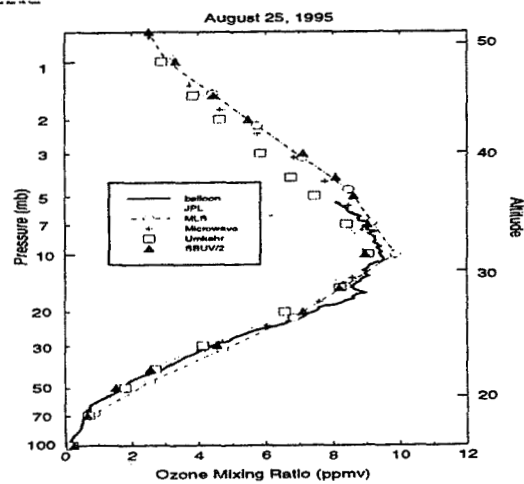


Figure 5. Ozone measurements during the NDSC campaign.

Also compared in this data set are data from the MLS on the UARS. The agreement of all the data sets with SBUV/2 is about 5% or better. Radiances were calculated using the method described above using the SBUV/2 ozone values illustrated in Figure 5. A total of six GOME observations near Mauna Loa from Channels 1a and 2 were compared to the calculated radiances of August 25. The radiance residuals are illustrated in figure 6. In

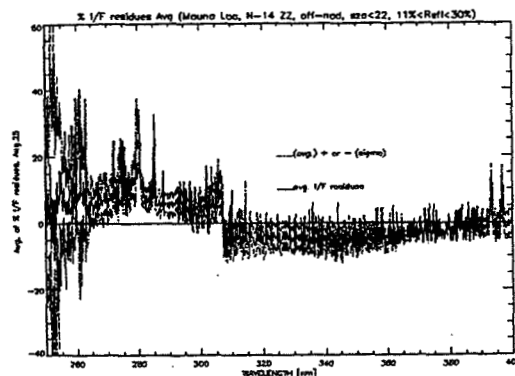


Figure 6. GOME and calculated radiances channels 1a and 2.

channel 1a, GOME measured radiances are about 10% higher on average.

The 1 sigma standard deviation grow to as large as $\pm 20\%$ but is likely due to GOME channel 1 detector noise. However, on average the GOME radiances are about 2% lower in channel 2 which is consistent with the results in Figure 2. The Ring effect, which was not removed in this comparison (because it was not modeled below 300 nm), results in sharp features at the Mg and Ca Fraunhofer lines seen in the Figure 6.

DOAS vs TOMS Total Ozone Retrievals

The Goddard UV algorithms were used for calculating total column ozone using GOME radiance and irradiance data. The GOME data was slit-averaged to TOMS 1.1 nm bandpass and the radiance and irradiance values interpolated to TOMS wavelengths at 312, 317, 331, 340, 360, 380 nm. Albedos, geo-location, solar zenith angles, satellite view angles were then processed through the version 7 TOMS algorithm (McPeters, et al 1993). The TOMS results were compared with DOAS results from the same ground pixel. The TOMS results were calculated with two different sets of wavelengths, the A-triplet: 312,331,380 nm, and the B-triplet: 316,331,380 nm. The primary difference between the triplets is the 312 wavelength of the A-triplet is measured using the 1b band radiances. All of the other wavelengths are measure in the 2b band. The differences between the A-triplet and the B-triplet ozone values are a measure of the inter-band calibration.

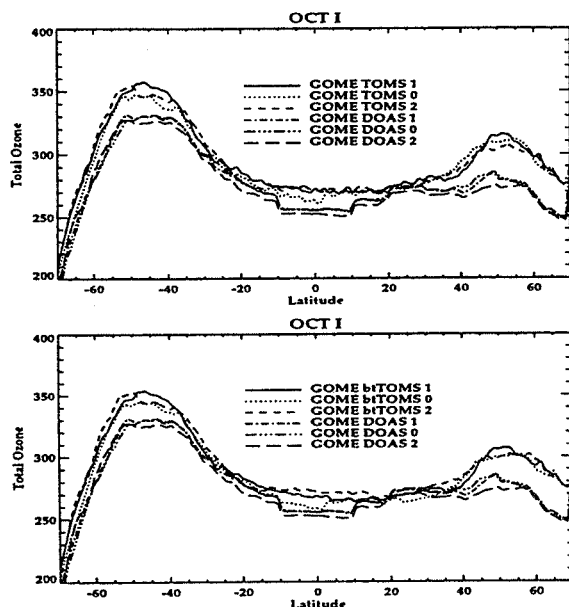


Figure 7. GOME-TOMS and GOME-DOAS ozone.

Figures 7 upper (A-triplet) and lower (B-triplet) show that the overall agreement between GOME-TOMS and the GOME-DOAS is reasonable. However the GOME-DOAS results are consistently lower than the TOMS results. The GOME-DOAS ozone values show a 'step function' behavior when plotted as a function of latitude. This behavior is probably the results of retrieval assumptions in the GOME-DOAS algorithm. Figure 8 upper (A-triplet) and lower (B-triplet) show the per-cent difference between the GOME-DOAS and the GOME-TOMS values as a function of latitude. The individual measurements have been smoothed for easier interpretation. Lower figure 8 shows a 2% positive shift compared with upper figure 8. This indicates a small calibration bias between the 312 nm radiance measured on Band 1b compared with the 317 nm radiances measured on Band 2b.

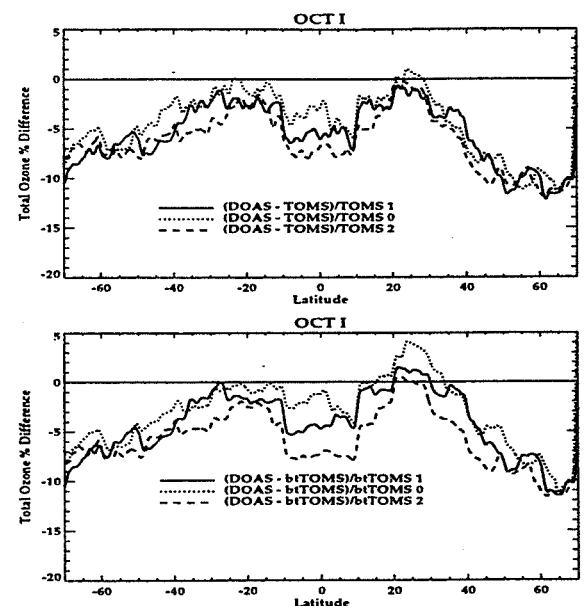


Figure 8. TOMS - DOAS differences versus latitude.

GOME-TOMS - GOME-DOAS differences show a significant (0 to 10%) latitude dependence. This is more likely a solar zenith angle dependence which is shown in figure 9 which is a replot of the data in figure 8. As the TOMS algorithm has not shown this solar zenith angle dependence using the Nimbus-7 radiance data, one must assume that this solar zenith angle (SZA) dependence is contained in the GOME-DOAS data. The other notable feature is the scan angle dependence of the GOME-TOMS results. The initial results presented at the final validation workshop in March, 1996 were calculated with incorrect SZA values. (NB: The SZA values recorded on the level 2 data records are the spacecraft SZA, not the SZA at the earth observation point!!) After this error was discovered the ozone values were recalculated and the scan bias was reduced but not removed. Further studies are required to assess the cause of this scan angle bias.

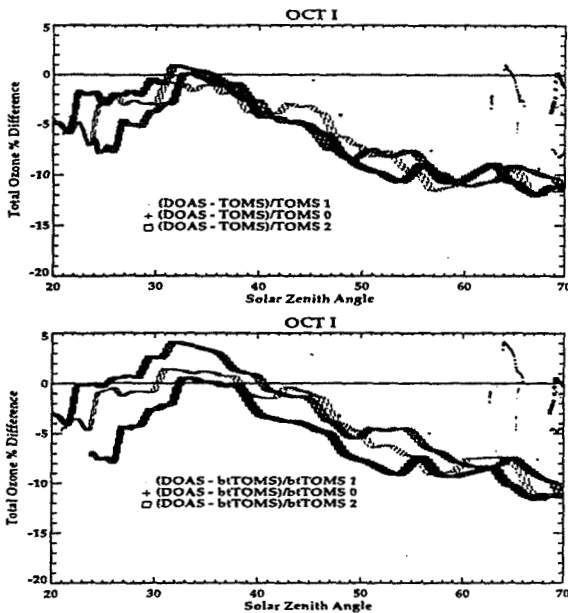


Figure 9. TOMS- DOAS differences versus SZA.

GOME Ozone Profiles Using the SBUV Algorithm

The Goddard algorithms were also used for calculating ozone vertical profiles using GOME radiance and irradiance data. The GOME data were again slit-averaged to the 1.1 nm SBUV bandpass. The radiance and irradiance data were interpolated to the 12 SBUV wavelengths; 255.5, 273.5, 283.0, 287.6, 292.2, 297.5, 301.9, 305.8, 312, 317, 331, 340 nm. Albedos, geo-location, solar zenith angles, and satellite view angles were processed through the version 6 SBUV algorithm.

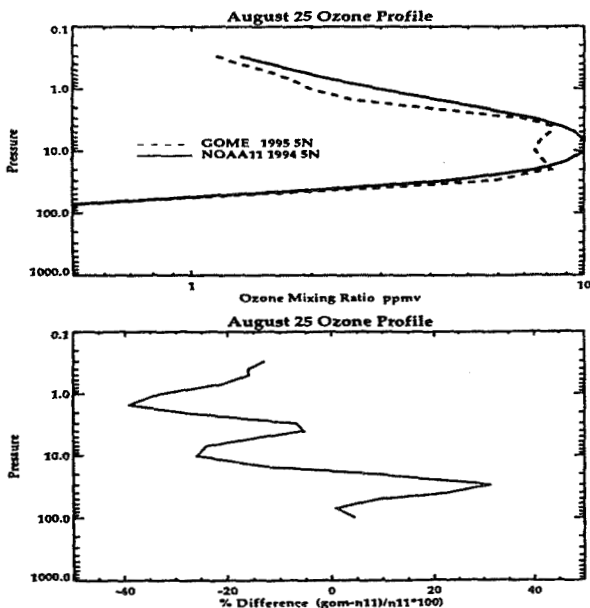


Figure 10. GOME profile results.

Approximately 130 measurements were averaged. The GOME 1996 average profile is compared to the same day

in 1995 measured by the SBUV/2 instrument on NOAA-11 and illustrated in the upper panel in figure 10. The GOME ozone profiles show too little ozone indicating that the radiance levels are too high. There is a notch in the profile at 10 mb indicating a wavelength dependent calibration error. The lower panel in figure 10 illustrates the difference in the GOME average profile and the climatology. Differences increase to as much as 30% near 1 mb. These results are consistent with the results described above in the Earth Radiance Comparison section. A 1% calibration error results in 2% ozone error at 1 mb. This ratio decreases with increasing pressure [Fleig et al., 1990].

Concluding Remarks

The NASA Goddard validation effort began before launch of GOME. NASA standards used for calibrating SBUV/2 and TOMS were also used to calibrate GOME. These calibrations were compared with TPD calibration and good agreement was found. The good agreement among the various calibration techniques and set-ups provides a large degree of confidence that the GOME instrument and the US BUV instruments are on a common radiometric scale, traceable to NIST standards, and provide a solid baseline for inter-comparisons of these instruments while in space.

Because TOMS Earth Probe launch is delayed, SBUV/2 has only recently become operational, and the SSBUV just completed its flight (January 11-18, 1996) after this first release of GOME data for validation, comparisons with Level 1 and 2 data has been limited. Nevertheless a great deal has been learned about the performance of GOME. Level 1 irradiance comparison show that GOME experienced a large wavelength dependent change in sensitivity as a result of the vacuum of space and is of the order of 15% at 300 nm. Level 1 radiances seem to agree with SBUV/2 calculated radiances on the order of a 2% at wavelengths larger than 340 nm. At wavelengths shorter than 300, GOME radiances appear to be high by as much as 10% with a large amount of noise. When comparing GOME DOAS total ozone values with GOME total ozone values using the BUV algorithm, a latitude and SZA angle dependence appears of the order of 0-10% where TOMS values are higher. GOME ozone profiles derived from the BUV profile algorithm compared with climatological values for the same season and latitude yields values about 10-30 % to low which is consistent with the Earth radiance difference discussed above. The irradiance error which results from the air-to-vacuum sensitivity change likely appears in the radiance as well. If this is the case, this error is canceled in the albedos and has no effect on retrievals. Therefore the error seen in the radiance (in reality albedo) from the SBUV comparisons below 300 does not seem to be a calibration error, but an

error associated with the key data applied to radiances in channel 1a. The source of the error is still unknown.

Algorithm research using GOME radiances has begun. Initial studies included studies of Ring data and relationship to cloud top heights, but are not reported here. GOME radiances between 340 and 400 which is free from ozone absorption were used to further study reflectivity anomalies discovered in TOMS which are associated with absorbing aerosols such as smoke and dust. With this initial release of GOME data one can conclude that these signatures likely also appear in the GOME radiances however further validation is required to draw any conclusions at this time.

It is recommended that pre-launch instrument key data particularly the air-to-vacuum shift be further refined. In addition, instrument performance should be tracked and corrected over time for the duration of its lifetime. This should be the primary objective for the GOME validation community. Instrument characteristics need to be updated periodically and Level-1 data products reprocessed. These data should then be validated followed by Level-2 reprocessing. Level-2 validation may reveal additional errors on either or both Level 1 and Level 2 data. This process is highly iterative and requires a team of committed and strongly supported experts to test and validate GOME data.

References

- Cebula, R. P., G. O. Thuillier, M. E. VanHoosier, E. Hilsenrath, M. Herse, G. E. Brueckner, and P. C. Simon, Observations of the solar irradiance in the 200-350 nm interval during the ATLAS-1 Mission: A comparison among three Sets of measurements - SSBUV, SOLSPEC, and SUSIM, *Geophys. Res. Lett.*, in press, 1996.
- Dave, J.V., Multiple scattering in a non-homogeneous, Rayleigh atmosphere, *J. Atmos. Sci.*, 22, 273-279, 1964
- Fleig, A.J., R.D. McPeters, P.K. Bhartia, B.M. Schlesinger, R.P. Cebula, K.F. Klenk, and S.L. Taylor, Nimbus-7 SBUV users guide, NASA Ref. Pub. 1234, 1990.
- Gu, X., R. D. McPeters, C. Seftor, C. Wellemeyer and R. P. Cebula, Spectral anomalies in the SBUV continuous scan data and validation of forward model calculation for ozone retrieval, to be submitted to *J. Geophys. Res.*, 1996.
- Hahne, A., J. Callies, A. Lefebvre, B. Christensen, R. Hoekstra, L. Fontijn, C. Olij, E. Zoutman, and G. Nutz, Calibration of the GOME instrument for ERS-2, *ESA Journal*, 18, 119-128, 1994.
- Heath, D.F., Z. Wei, W.K. Fowler, and V.W. Nelson, Comparison of spectral radiance calibrations of SBUV-2 satellite ozone monitoring instruments using integrating sphere and flat-plate diffuser techniques, *Metrologia*, 30, 259-264, 1993
- Heath, D.F., R. Hoekstra, E. Zoutman, C. Olij, "NASA Sphere Calibration for GOME FM", TPD-ERS-GO-MIR-33, 1994.
- Hilsenrath, E., P.K. Bhartia, and R.P. Cebula, Calibration of BUUV satellite ozone data - An example of for detecting environmental trends, *Earth Observer*, 6, 26-33, 1994
- Hsu, C., J.R. Herman, P.K. Bhartia, C.J. Seftor, O. Torres, A.M. Thompson, J.F. Gleason, T.F. Eck, and B.N. Holben, Detection of biomass burning smoke from TOMS measurements, *Geophys. Res. Lett.* 23, 745-748, 1996.
- Janz, S., E. Hilsenrath, J. Butler, D.F. Heath and R.P. Cebula, Uncertainties in radiance calibrations of backscatter ultraviolet (BUV) instruments, *Metrologia*, (in press), 1996.
- Joiner, J., P. K. Bhartia, R. P. Cebula, E. Hilsenrath, R. D. McPeters, and H. Park, Rotational Raman scattering (RING effect) in satellite Backscatter ultraviolet measurements, *Appl. Opt.*, 34, 4513-4525, 1995.
- McPeters, R.D., A.J. Krueger, P. K. Bhartia, J.R. Herman, A. Oaks, Z. Ahmad, R. P. Cebula, B.M. Schlesinger, T. Swisler, S.L. Taylor, O. Torres, C.G. Wellemeyer, Nimbus-7 Total Ozone Mapping Spectrometer (TOMS) Data Products User's Guide, NASA reference Publication 1323, 1993
- Torres, O. and P.K. Bhartia, Effect of stratospheric aerosol on ozone profile from BUUV measurements, *Geophys. Res. Lett.* 22, 235-238, 1995.
- Woods, T. N., D. K. Prinz, J. London, G. J. Rottman, P. C. Crane, R. P. Cebula, E. Hilsenrath, G. E. Brueckner, M. D. Andrews, O. R. White, M. E. VanHoosier, L. E. Floyd, L. C. Herring, B. G. Knapp, C. K. Pankratz, and P. A. Reiser, Validation of the UARS and ATLAS Solar ultraviolet irradiances, *J. Geophys. Res.*, in press, 1996.

Acknowledgements

We thank Richard McPeters of Goddard Space Flight Center who provided us with advance data from the NDSC intercomparison.